

Sensor and Simulation Notes

Note 158

November 1972

The Effect of Flanges on the Inductance of a Sloped
Termination for a Parallel-Plate Simulator

M. I. Sancer and A. D. Varvatsis
Northrop Corporate Laboratories
Pasadena, California

CLEARED
FOR PUBLIC RELEASE
PL/PA 5/19/97

Abstract

The value of the inductance for the termination of a parallel-plate simulator has previously been chosen on the basis of an analysis which considered coplanar flanges to extend beyond the terminating admittance sheet. The flanges were introduced to facilitate that analysis, the underlying assumption being that the solution with the flanges is not significantly different from the solution without the flanges. In this note we test this assumption by using a wedge Green's function that allows us to vary the angle of one flange while the other remains coplanar. We find that the effect of coplanar flanges is small if we compare that case to the case where the flanges are alternately removed; however, there is a flange orientation of interest that can make a considerable difference in the choice of the inductance. This orientation corresponds to the simulator resting on a perfectly conducting ground. Our results are summarized in a table of normalized inductance values for various slope angles of the terminating admittance sheet as well as various physically significant flange orientations for each slope angle. We also present the appropriate graphs that lead to this choice of inductance values.

PL 96-1219

I. Introduction

The value of the inductance for the termination of a parallel-plate simulator is now being chosen on the basis of previous results [1]. In [1], flanges were considered to be present in order to facilitate the analysis. The underlying assumption is that the solution with flanges is not significantly different from the solution without flanges. We have completed a study that allows us to test this assumption.

Our analysis is based on the use of the Green's function for the perfectly conducting wedge. The use of this Green's function allows one to vary the angle of either the top or the bottom flange, with the other flange remaining coplanar with the termination. We have calculated the time dependent ideal current that would exist on a perfect termination (no reflections) if it had a step function TEM wave incident upon it. We calculate and plot this current versus an appropriate normalized time scale with the quantities ξ , δ , and α serving as parameters for each plot. The meaning of these quantities is as follows: ξ is the angle between the termination plane and the bottom plate of the simulator, δ an angle that defines the orientations of a flange, and α is the ratio of the distance from the intersection of the termination plane and the top plate of the simulator divided by the length of the termination plane. (See figure 1).

Once the ideal current is determined, we compare it to the approximate current that would exist in an R, L admittance sheet. The value of R that is used in this admittance sheet is fixed from a late time argument that is independent of flange considerations; however, the value of L is chosen so that the approximate current behaves as much as possible like the ideal current for a certain required period of time.

Our results show that Baum's assumption concerning the insignificant effect of coplanar flanges on the ideal current in the termination is valid if we compare that case to the case where the flanges are alternately removed; however, there is a flange orientation of interest that can make a considerable difference in the choice of L. This is the case corresponding to an orientation of the bottom flange so that it is an extension of the bottom plate of the simulator. This orientation corresponds to a vertically polarized simulator

resting on a perfectly conducting ground. For this orientation of the flange and $\xi = 90^\circ$, the value of L one should choose is approximately twice the value of L one would obtain in matching the ideal current if the bottom flange were absent corresponding to a nonconducting ground. The difference in the value of L one should use for these two extreme cases diminishes as ξ diminishes. This is another reason for using sloped terminations. Another way of diminishing the effect of the ground conductivity on the value of inductance was found by considering a flange angle corresponding to removing and sloping the ground beyond the simulator.

Our results are summarized in tables of normalized inductance values for various ξ , δ orientations. We also present the curves of the ideal and approximate currents which led to this choice of inductance values.

II. Ideal Current When Angle of Bottom Flange is Varied

The analysis of the effect due to varying the angle of the bottom flange is facilitated by considering figure 1. Later we will discuss how this analysis can be used to consider the effect of varying the angle of the top flange.

In region 1, H_z satisfies the equation

$$(\nabla_0^2 + k^2)H_z = 0 \quad (1)$$

where ∇_0^2 is the two dimensional Laplacian operator and k is the free space wave number. We will also use the Green's function that satisfies the equation

$$(\nabla_0^2 + k^2)G = \delta(\underline{\rho} - \underline{\rho}_0) \quad (2)$$

in region 1 as well as boundary conditions corresponding to the wedge being perfectly conducting. This G is found by making use of the scattering solution contained in the book by Bowman, Senior, and Uslenghi [2] when the incident field is due to a line source. That is

$$H_{zi} = \hat{a}_z H_0^{(1)}(k|\underline{\rho} - \underline{\rho}_0|) \quad (3)$$

For this incident field, G is given by

$$G(\underline{\rho}, \underline{\rho}_0) = \frac{i}{4} H_{zLS} \quad (4)$$

where H_{zLS} is the total field, incident plus scattered field, when H_{zi} given by (3) strikes the wedge depicted in figure 1 with the termination considered to be perfectly conducting. Using the notation in [2], this quantity is given by

$$H_{zLS} = H_z^{G.O.} + H_z^D \quad (5)$$

where

$$H_z^{G.O.} = \sum_{n_1} H_0^{(1)}[kR(\alpha_{n_1})] + \sum_{n_2} H_0^{(1)}[kR(\alpha_{n_2})] \quad (6)$$

$$\alpha_{n_1} = \pi - \phi + \phi_0 - 2n_1 v \pi \quad (7)$$

$$\alpha_{n_2} = \pi - \phi - \phi_0 + 2\Omega - 2n_2 v \pi \quad (8)$$

$$R(\alpha) = (\rho^2 + \rho_0^2 + 2\rho\rho_0 \cos \alpha)^{\frac{1}{2}} \quad (9)$$

$$v = 2\left(1 - \frac{\Omega}{\pi}\right) \quad (10)$$

and the summation is over the positive integers n_1 and n_2 satisfying the inequalities

$$|\phi - \phi_0 + 2n_1 v \pi| \leq \pi \quad (11)$$

and

$$|\phi + \phi_0 - 2\Omega + 2n_2 v \pi| \leq \pi \quad (12)$$

where further

$$\begin{aligned} H_z^D &= V_D(-\pi - \phi + \phi_0) - V_D(\pi - \phi + \phi_0) \\ &+ V_D(-\pi - \phi - \phi_0 + 2\Omega) - V_D(\pi - \phi - \phi_0 + 2\Omega) \end{aligned} \quad (13)$$

$$V_D(\beta) = \frac{1}{2\pi v} \int_0^\infty H_0^{(1)}[kR(ip)] \frac{\sin \beta v}{\cosh(p/v) - \cos(\beta/v)} \quad (14)$$

$$R(ip) = (\rho^2 + \rho_0^2 + 2\rho\rho_0 \cosh p)^{\frac{1}{2}} \quad (15)$$

For the case of interest $\phi = \phi_0 = \Omega$ and the expression for $G(\rho, \rho_0)$ reduces to

$$G(\rho, \rho_0) = -\frac{i}{2} H_0^{(1)}(k|\rho - \rho_0|) + \frac{i}{2\pi v} \sin \frac{\pi}{v} \int_0^\infty H_0[kR(ip)] \frac{dp}{\cosh(p/v) - \cos(\pi/v)} \quad (16)$$

We now use $G(\rho, \rho_0)$ in the Green's theorem

$$\int_A [H_z \nabla_0^2 G - G \nabla_0^2 H_z] dS_0 = \int \hat{n} \cdot [H_z \nabla_0 G - G \nabla_0 H_z] d\ell_0 \quad (17)$$

and (1) and (2) in order to arrive at

$$H_z(\rho) = - \int_0^d G(\rho, \rho_0) (\hat{n} \cdot \nabla_0 H_z) d\rho_0 \quad (18)$$

The area over which we integrated in (17) is depicted in figure 1. It is the area bounded by the wedge having an angle 2Ω and the dashed contour. The differential arclength, $d\ell_0$, as well as the outward normal, \hat{n} , are also depicted. We also made use of the facts that $\hat{n} \cdot \nabla_0 H_z$ vanishes on the conducting portion of the wedge while $\hat{n} \cdot \nabla_0 G$ vanishes on the entire wedge. Both of these quantities vanish sufficiently fast at infinity so that the contour integral vanishes at infinity.

We now simplify (18) further by noting that

$$\hat{n} \cdot \nabla_0 H_z = i\omega \epsilon_0 E_{\rho_0} \quad (19)$$

and that

$$E_{\rho_0} = E_y \sin \xi \quad (20)$$

so that

$$H_z(\rho) = \int_0^d G(\rho, \rho_0) \sin \xi \epsilon_0 F \left[\frac{\partial E_y}{\partial t} \right] d\rho_0 \quad (21)$$

where F indicates the Fourier transform. Equation (21) is our desired equation for both the source and termination problem. The main difference in these problems is the specification of $E_y(\rho_0, t)$ along the plane which corresponds to either a distributed source sheet or distributed termination.

In the derivation of (16) we implicitly used the fact that the only integers which satisfy (11) and (12) were $n_1 = n_2 = 0$. Both (11) and (12) are simplified to

$$|n_1(2\pi - 2\Omega)| \leq \pi \quad (22)$$

and

$$|n_2(2\pi - 2\Omega)| \leq \pi \quad (23)$$

The largest value that 2Ω can have for the flange angles of interest is $3\pi/2$ and for this case n_1 and n_2 can each equal 1. This is the case only when $\xi = \pi/2$ and the bottom flange corresponds to an extension of the bottom plate of the simulator. This corresponds to the case where the simulator is resting on a perfectly conducting ground. This particular case yields a closed form analytical solution and will be treated in another section of this note.

We now consider the case of the termination problem where the angle of the bottom flange is varied. This case will be treated in detail and the other cases will make use of the analysis for this case. The electric field that is substituted into (21) is

$$\frac{E}{-y} = -\hat{a}_y E_0 U(t - \frac{v_0}{c} \cos \xi) \quad (24)$$

This corresponds to the electric field of the incident TEM mode that is propagating between the parallel plates of the simulator. Since we are considering a perfect termination, this is the total electric field on the termination sheet because the reflected field is zero. The quantity, v_0 , is the distance measured along the termination from the top junction and $t = 0$ when the incident wave first strikes this junction. Substituting (24) into (21) we have

$$H_z(\rho, \omega) = -\epsilon_0 E_0 \sin \xi \int_0^d d\rho_0 G(\rho, \rho_0) F[\delta(t - \frac{v_0}{c} \cos \xi)] \quad (25)$$

We are interested in the time dependent solution for H_z . This is obtained by taking the inverse Fourier transform of (25). That is

$$H_z(\rho, t) = -\epsilon_0 E_0 \sin \xi \int_0^d d\rho_0 \hat{G}(\rho, \rho_0, t) * \delta(t - \frac{v_0}{c} \cos \xi) \quad (26)$$

where * indicates time domain convolution. Returning to (16) we write

$$G(\rho, \rho_0) = G_1(\rho, \rho_0) + G_2(\rho, \rho_0) \quad (27)$$

where

$$G_1(\rho, \rho_0) = -\frac{i}{2} H_0^{(1)}[k|\rho - \rho_0|] \quad (28)$$

and

$$G_2(\rho, \rho_0) = \frac{i \sin(\pi/v)}{2\pi v} \int_0^\infty dp \frac{H_0^{(1)}[kR(ip)]}{\cosh(p/v) - \cos(\pi/v)} \quad (29)$$

In the time domain these quantities become

$$\hat{G}_1(\rho, \rho_0, t) = \frac{1}{2} \pi \int_{-\infty}^\infty G_1(\rho, \rho_0) e^{-i\omega t} d\omega \quad (30)$$

$$\hat{G}_1(\rho, \rho_0, t) = -\frac{c}{\pi} \frac{U(ct - |\rho - \rho_0|)}{\sqrt{(ct)^2 - (\rho - \rho_0)^2}} \quad (31)$$

and similarly

$$\hat{G}_2(\rho, \rho_0, t) = \frac{c \sin(\pi/v)}{v\pi^2} \int_0^\infty \frac{U(ct - R(ip))}{\sqrt{(ct)^2 - R^2(ip)}} \frac{dp}{\cosh(p/v) - \cos(\pi/v)} \quad (32)$$

where $c = (\mu_0 \epsilon_0)^{-1/2}$ and U is a step function. In order to obtain (31) and (32) we used the following relation which can be found in the book by Morse and Feshbach[3] or in a note by Baum [4]. That is

$$\int_{-\infty}^\infty H_0^{(1)}(kR) e^{-i\omega t} d\omega = -4ci \frac{U(ct - R)}{\sqrt{(ct)^2 - R^2}} \quad (33)$$

Now we use (31) and (32) to define H_{z_1} and H_{z_2} as

$$H_z(\rho, t) = H_{z_1}(\rho, t) + H_{z_2}(\rho, t) \quad (34)$$

where

$$H_{z_1}(\rho, t) = \frac{E_o}{\pi Z_o} \sin \xi \int_0^d d\rho_o \frac{U(ct - |\rho - \rho_o|)}{\sqrt{(ct)^2 - (\rho - \rho_o)^2}} * \delta\left(t - \frac{d - \rho_o}{c} \cos \xi\right) \quad (35)$$

$$H_{z_1} = \frac{E_o}{\pi Z_o} \sin \xi \int_0^d d\rho_o \frac{U[ct - (d - \rho_o) \cos \xi - |\rho - \rho_o|]}{\sqrt{(ct - (d - \rho_o) \cos \xi)^2 - (\rho - \rho_o)^2}} \quad (36)$$

similarly

$$H_{z_2} = -\frac{E_o}{\pi^2 Z_o v} \sin(\pi/v) \sin \xi I_2 \quad (37)$$

where

$$I_2 = \int_0^\infty \frac{dp}{\cosh(p/v) - \cos(\pi/v)} \int_0^d d\rho_o \frac{U[ct - (d - \rho_o) \cos \xi - R(ip)]}{\sqrt{(ct - (d - \rho_o) \cos \xi)^2 - R^2(ip)}} \quad (38)$$

We have used the relations $Z_o = (\mu_o/\epsilon_o)^{1/2}$ and $v_o = d - \rho_o$. H_{z_1} will be evaluated by casting it in a form that was treated in detail in a previous note by Baum [1]. If we rewrite (36) using $v = d - \rho$ and again $v_o = d - \rho_o$ as

$$H_{z_1} = \frac{E_o}{\pi Z_o} \sin \xi \int_0^d \frac{dv_o}{|v - v_o|} \frac{U[ct - v_o \cos \xi - |v - v_o|]}{\{((ct - v_o \cos \xi)/|v - v_o|)^2 - 1\}^{1/2}} \quad (39)$$

then we can identify our H_{z_1} as

$$H_{z_1} = -\frac{E_o}{Z_o} [j_{s_1} + j'_{s_2}] \quad (40)$$

or

$$H_{z_1} = \frac{E_o}{Z_o} [U(\tau) - j_{s_4}] \quad (41)$$

We will not define j_{s_1} or j'_{s_2} here; they were only mentioned to facilitate the comparison of the integral contained in (39) with the explicit integrals evaluated by Baum. The quantity j'_{s_4} (Baum's notation) is now implicitly defined by expressing (41) as

$$H_{z_1}(\rho, t) = \frac{E_0}{Z_0} \left[U(\tau) - \frac{1}{\pi} U(\tau - \tau_1) \arccos \left[\frac{\alpha \sin \xi - \tau \cos \xi}{\tau} \right] \right. \\ \left. - \frac{1}{\pi} U(\tau - \tau_2) \arccos \left[\frac{(1-\alpha) \sin \xi + \tau \cos \xi}{\tau} \right] \right] \quad (42)$$

where

$$\tau = \frac{ct - v \cos \xi}{d \sin \xi} \quad (43)$$

$$\tau_1 = \alpha \frac{1 - \cos \xi}{\sin \xi} \quad (44)$$

$$\tau_2 = (1 - \alpha) \frac{1 + \cos \xi}{\sin \xi} \quad (45)$$

$$\alpha = v/d = 1 - \rho/d \quad (46)$$

We now return to $H_{z_2}(\rho, t)$ and we will cast (38) into a form that can be better handled analytically and numerically. I_2 is of the form

$$I_2 = \int_0^\infty dp \int_0^d d\rho_0 F(p, \rho_0) U[T + a\rho_0 - R] \quad (47)$$

where

$$T = ct - ad \quad (48a)$$

$$a \equiv \cos \xi \quad (48b)$$

$$F = A(p) ((T + a\rho_0)^2 - R^2)^{-1/2} \quad (48c)$$

$$A(p) = (\cosh(p/v) - \cos(\pi/v))^{-1} \quad (48d)$$

We write I_2 in this form so that we can concentrate on determining the appropriate limits of integration that would allow us to eliminate the unit step function in (47). The arguments concerning how this is accomplished can be understood by referring to figure 2. The region that the original integration is to be taken over in (47) is the semi-infinite rectangle $0 \leq \rho_0 \leq d$ and $p \geq 0$. Depicted in figure 2 are plots of ρ_0 versus p corresponding to the argument of the step

function equal to zero. That is

$$T + a\rho_0 - R = 0 \quad (49)$$

The explicit function that is depicted is

$$\rho_0(p, T) = \frac{Ta - \rho b + \{(Ta - \rho b)^2 + (1 - a^2)(T^2 - \rho^2)\}^{\frac{1}{2}}}{1 - a^2} \quad (50)$$

where

$$b = \cosh p \quad (51)$$

Two important values of $\rho_0(p, T)$ are

$$\rho_0(\infty, T) = 0 \quad (52)$$

and

$$\rho_0(0, T) = \frac{T - \rho}{1 - a} \quad \text{for } T > \rho \quad (53)$$

The largest value that $\rho_0(p, T)$ can have is $\rho_0(0, T)$. To see this, we consider the derivative

$$\frac{\partial \rho_0(p, T)}{\partial p} = - \frac{\rho \sinh p}{\sin^2 \xi} [1 - M] \quad (54)$$

where

$$M = \frac{(\rho b - Ta)}{|\rho b - Ta|} (1 + \sin^2 \xi (T^2 - \rho^2) / (\rho b - Ta)^2)^{-\frac{1}{2}} \quad (55)$$

Since we will be interested only in the case $T > \rho$ we can see that

$$|M| < 1$$

Referring back to (54) and adding the requirement $\rho \neq 0$, we see that

$$\frac{\partial \rho_0(p, T)}{\partial p} < 0 \quad \text{for } p > 0 \quad (56)$$

Thus, $\rho_o(p,T)$ is a monotonically decreasing function of p for any T . This implies that the curve $\rho_o(p,T)$ versus p will never cross the line $\rho_o = d$ if $\rho_o(0,T) < d$ and this curve will cross the $\rho_o = d$ line only once if $\rho_o(0,T) > d$. The case $\rho = 0$ will be treated separately in the next section. What is left to determine is whether we should integrate over the intersection of our original semi-infinite rectangle and the area above the $\rho_o(p,T)$ curve or the intersection with the area below the $\rho_o(p,T)$ curve. To settle this point we need only examine the value of the function $T + a\rho_o - R$ at the origin. We find

$$T + a\rho_o - R = T - \rho > 0 \quad \text{for } \rho_o = p = 0 \quad (57)$$

Thus the area over which we integrate is the intersection of the rectangle $0 \leq \rho_o \leq d$, $0 \leq p$ with the area below the $\rho_o(p,T)$ curve. There are now two cases to consider. They are

$$0 < \rho_o(0,T) \leq d \quad (58)$$

and

$$\rho_o(0,T) \geq d \quad (59)$$

Using (53) and (48a), these conditions become

$$\rho + ad < ct \leq d + \rho \quad (58)$$

and

$$ct \geq d + \rho \quad (59)$$

When condition (58) is satisfied, then (47) becomes

$$I_2 = [U(ct - (\rho + ad)) - U(ct - (\rho + d))] \int_0^\infty dp \int_0^{\rho_o(p,T)} d\rho_o F(p, \rho_o) \quad (60)$$

When condition (59) is satisfied, then we must solve for the value of p corresponding to the point where the $\rho_o(p,T)$ curve intersects the $\rho_o = d$ line.

This value of p_I must be found before we can set the appropriate limits for the evaluation of I_2 . Setting

$$\rho_o(p_I, T) = d \quad (61)$$

and solving for p_I , we obtain

$$p_I = \operatorname{arccosh} \left[1 + \frac{(ct)^2 - (\rho+d)^2}{2\rho d} \right] \quad (62)$$

We can now write (47) as

$$I_2 = U(ct - (\rho + d)) \int_0^{p_I} dp \int_0^d d\rho_o F(p, \rho_o) + \int_{p_I}^{\infty} dp \int_0^{\rho_o(p, T)} d\rho_o F(p, \rho_o) \quad (63)$$

Using (48), the three integrals in (60) and (63) can be written as

$$I_3 = \int_0^{\infty} dp \int_0^{\rho_o(p, T)} d\rho_o F(p, \rho_o) = \int_0^{\infty} dp A(p) I_6 \quad (64)$$

$$I_4 = \int_0^{p_I} dp \int_0^d d\rho_o F(p, \rho_o) = \int_0^{p_I} dp A(p) I_7 \quad (65)$$

$$I_5 = \int_{p_I}^{\infty} dp \int_0^{\rho_o(p, T)} d\rho_o F(p, \rho_o) = \int_{p_I}^{\infty} dp A(p) I_6 \quad (66)$$

where

$$I_6 = \int_0^{\rho_o(p, T)} d\rho_o ((T + a\rho_o)^2 - R^2)^{-\frac{1}{2}} \quad (67)$$

and

$$I_7 = \int_0^d d\rho_o ((T + a\rho_o)^2 - R^2)^{-\frac{1}{2}} \quad (68)$$

The integrals I_6 and I_7 can readily be evaluated in terms of inverse trigonometric functions. The resulting evaluations are

$$I_6 = (\sin \xi)^{-1} \operatorname{arccos}(\rho b - Ta) / ((\rho b - Ta)^2 + (1 - a^2)(T^2 - \rho^2))^{\frac{1}{2}} \quad (69)$$

$$I_7 = (\sin \xi)^{-1} \left[\arcsin((1 - a^2)d + \rho b - Ta) / ((\rho b - Ta)^2 + (1 - a^2)(T^2 - \rho^2))^{\frac{1}{2}} \right. \\ \left. - \arcsin(\rho b - Ta) / ((\rho b - Ta)^2 + (1 - a^2)(T^2 - \rho^2))^{\frac{1}{2}} \right] \quad (70)$$

This is as far as we can evaluate I_3 , I_4 , and I_5 analytically. In order to facilitate their numerical evaluation we make the following change of variables.

$$y = e^{-P} \quad (71)$$

This enables us to eliminate the infinite limit of integration. We are now in a position to present the explicit form for the current in the final form that was numerically integrated.

The surface current density on the termination sheet, J , is defined as

$$J = H_z^{\text{TEM}} - H_z(\rho, t) \quad (72)$$

This definition uses the fact that we are considering a perfect termination so that the total magnetic field on the simulator side of the termination is just the incident field. Recall that

$$H_z(\rho, t) = H_{z_1}(\rho, t) + H_{z_2}(\rho, t)$$

and that $H_{z_1}(\rho, t)$ is defined in (42) through (46), while $H_{z_2}(\rho, t)$ is defined in (38) in terms of I_2 . Subsequently I_2 has been defined in terms of I_3 through I_7 . From (24) we know that

$$H_z^{\text{TEM}} = \frac{E_o}{Z_o} U(t - \frac{v}{c} \cos \xi) \quad (73)$$

The final equation for the normalized surface current density, j , defined as

$$j = \frac{Z_o}{E_o} J \quad (74)$$

is

$$\begin{aligned}
j = & 1/\pi U(\tau - \tau_1) \arccos[\tau^{-1}(\alpha \sin \xi - \tau \cos \xi)] \\
& + 1/\pi U(\tau - \tau_2) \arccos[\tau^{-1}((1 - \alpha) \sin \xi + \tau \cos \xi)] \\
& + q/\pi^2 \sin q\pi \{ [U(\tau - \tau_2) - U(\tau - \tau_3)] I_A + U(\tau - \tau_3) I_B \}
\end{aligned} \tag{75}$$

where, repeating (43), (44), and (45)

$$\begin{aligned}
\tau &= \frac{ct - v \cos \xi}{d \sin \xi} \\
\tau_1 &= \frac{1 - \cos \xi}{\sin \xi} \alpha \\
\tau_2 &= (1 - \alpha) \frac{1 + \cos \xi}{\sin \xi}
\end{aligned}$$

and defining the remaining quantities in (75) as

$$\tau_3 = \tau_2 + \frac{1 - \cos \xi}{\sin \xi} \tag{76}$$

$$q \equiv 1/v = \pi / (\pi + \delta - \xi) \tag{77}$$

$$I_A = \int_0^1 A(y) \arccos g(y) dy \tag{78}$$

$$I_B \equiv I_{B_1} + I_{B_2} \tag{79}$$

$$I_{B_1} = \int_0^{y_I} A(y) \arccos g(y) dy \tag{80}$$

$$I_{B_2} = \int_{y_I}^1 A(y) \{ \arcsin [g(y) + e(y)] - \arcsin g(y) \} dy \tag{81}$$

$$A(y) = 2y^{q-1} / (y^{2q} - 2y^q \cos q\pi + 1) \tag{82}$$

$$g(y) = C(C^2 + D^2)^{-1/2} \tag{83}$$

$$C = y^2 - 2y\beta \cos \xi + 1 \quad (84)$$

$$D^2 = 4y^2(\beta^2 - 1)\sin^2\xi \quad (85)$$

$$e(y) = 2y \sin^2\xi / [(1 - \alpha)(C^2 + D^2)^{\frac{1}{2}}] \quad (86)$$

$$\beta = \tau \sin \xi / (1 - \alpha) - \cos \xi \quad (87)$$

$$y_{\perp} = 1 + \Gamma - ((1 + \Gamma)^2 - 1)^{\frac{1}{2}} \quad (88)$$

$$\Gamma = [(\beta(1 - \alpha) + \cos \xi)^2 - (2 - \alpha)^2] / [2(1 - \alpha)] \quad (89)$$

It should be noted that the first two terms in (75) represent the surface current density corresponding to coplanar flanges, while remaining terms correspond to the effect of bending the lower flange. We have now defined all of the terms (75) and this is the expression that is evaluated numerically to obtain the value of the ideal current in the perfect termination. Two situations are not described by (75) without considering a limiting process. They are the case where $\rho = 0$ and the orientation $\xi = \pi/2$, $\delta = 0$. The case $\rho = 0$ is not included because of (56) and case $\xi = \pi/2$, $\delta = 0$ is not included because n_1 and n_2 can each equal 1 and still satisfy (22) and (23). In obtaining (75) we have not included the contributions corresponding to $n_1 = n_2 = 1$. In the next two sections we will obtain analytic expressions for j for each of these two cases.

III. Analytic Evaluation of Current Density at the Bend

We now return to (38) and consider the case $\rho = 0$. We rewrite I_2 as

$$I_2 = \int_0^\infty \frac{dp}{\cosh qp - \cos q\pi} I_0 \quad (90)$$

where

$$I_0 = \int_0^d d\rho_0 \left\{ U \left[T + a\rho_0 - R \right] \left[(T + a\rho_0)^2 - R^2 \right]^{-\frac{1}{2}} \right\}_{\rho=0} \quad (91)$$

$$I_0 = \int_0^d d\rho_0 U \left[T - \rho_0(1-a) \right] \left[(T + a\rho_0)^2 - \rho_0^2 \right]^{-\frac{1}{2}}$$

First consider the case

$$0 < T \leq d(1-a) \quad (92)$$

Then

$$I_0 = \int_0^{T/(1-a)} d\rho_0 \left[(T + a\rho_0)^2 - \rho_0^2 \right]^{-\frac{1}{2}} \quad (93)$$

which can readily be evaluated to give

$$I_0 = (\pi - \xi) / \sin \xi \quad (94)$$

It is easy to see that (94) should be independent of T . Imagine that (93) was evaluated by making the change of variables $\rho_0 = Ty$. Then the T dependence would cancel in (93) in both the integrand and the limits of integration. We now consider the case

$$d(1-a) \leq T \quad (95)$$

For this case

$$I_0 = \int_0^d d\rho_0 \left[(T + a\rho_0)^2 - \rho_0^2 \right]^{-\frac{1}{2}} \quad (96)$$

$$I_0 = (1/\sin \xi) [\pi - \xi - \arccos[\tau^{-1}(\sin \xi - \tau \cos \xi)]] \quad (97)$$

where, using (43), (48a) and (48b) for $v = d$, ($\alpha = 1$), we see that

$$\tau = T/(d \sin \xi) \quad (98)$$

Returning to (90) we write

$$I_2 = I_2' I_0 \quad (99)$$

where

$$I_2' = \int_0^\infty dp (\cosh qp - \cos q\pi)^{-1} \quad (100)$$

This integral is readily evaluated by letting $e^{-qp} = y$. One then obtains a standard arctan integral, which after using several trigonometric identities yields the result

$$I_2' = [\pi/q (1 - q)]/\sin q\pi \quad (101)$$

Using (77), we can express this as

$$I_2' = (\delta - \xi)/\sin q\pi \quad (102)$$

Before we express our final result for I_2 we use (44) with $\alpha = 1$ as well as (98) to write conditions (92) and (95) as

$$0 < \tau \leq \tau_1 = \frac{1 - \cos \xi}{\sin \xi} \quad (103)$$

and

$$\tau_1 \leq \tau \quad (104)$$

Now combining the results of this section, the expression for I_2 can be written as

$$I_2 = \frac{\delta - \xi}{\sin \xi \sin q\pi} [U(\tau)[\pi - \xi] - U(\tau - \tau_1)\arccos(\tau^{-1}(\sin \xi - \tau \cos \xi))] \quad (105)$$

Noting (37), (72), (73) and (77), we see that the current corresponding to the bend, j' , is given by

$$j' = (q/\pi^2)\sin \xi \sin q\pi I_2 \quad (106)$$

which, using (77), can be written as

$$j' = \frac{1}{\pi} \frac{\delta - \xi}{\pi + \delta - \xi} \{U(\tau)(\pi - \xi) - U(\tau - \tau_1)\arccos(\tau^{-1}(\sin \xi - \tau \cos \xi))\} \quad (107)$$

The total j , including the coplanar contribution given by the first two terms in (75) with $\alpha = 1$, is

$$j = \frac{1}{\pi} \left\{ U(\tau) \left[\xi + \frac{(\delta - \xi)(\pi - \xi)}{\pi + \delta - \xi} \right] + U(\tau - \tau_1)\arccos(\tau^{-1}(\sin \xi - \tau \cos \xi)) \left(1 - \frac{\delta - \xi}{\pi + \delta - \xi} \right) \right\} \quad (108)$$

The coplanar j can readily be seen by noting the terms which remain in (108) after setting $\delta = \xi$.

IV. Analytic Evaluation of Current Density for $\xi = \pi/2$ and $\delta = 0$

For the special case $\xi = \pi/2$ and $\delta = 0$ we can satisfy (11) and (12) for $n_1 = n_2 = 1$. According to (6) this leads to a new definition for $H_Z^{G.O.}$. This quantity is now given by

$$H_Z^{G.O.} = 2H_0^{(1)}[k|\rho - \rho_0|] + 2H_0^{(1)}[k|\rho + \rho_0|] \quad (109)$$

For the angles ξ and δ considered in this section, $\nu = \frac{1}{2}$. The quantity H_Z^D contains a multiplicative factor $\sin(\pi/\nu)$ and consequently is equal to zero, so that using (4) and (5) we have

$$G(\rho, \rho_0) = -\frac{i}{2} H_0^{(1)}(k|\rho - \rho_0|) - \frac{i}{2} H_0^{(1)}(k|\rho + \rho_0|) \quad (110)$$

The corresponding time dependent Green's function is obtained by taking the inverse Fourier transform. Using (33) we obtain

$$\hat{G}(\rho, \rho_0, t) = \hat{G}_1(\rho, \rho_0, t) + \hat{G}_3(\rho, \rho_0, t) \quad (111)$$

whereas in section II, $\hat{G}_1(\rho, \rho_0, t)$ is the inverse transform of the first term in (110) and is given in (31). The quantity, $\hat{G}_3(\rho, \rho_0, t)$ is the inverse transform of the second term in (109) and is given by

$$\hat{G}_3(\rho, \rho_0, t) = -c/\pi((ct)^2 - (\rho + \rho_0)^2)^{-\frac{1}{2}} U(ct - \rho - \rho_0) \quad (112)$$

Equation (26) is valid for $\hat{G}(\rho, \rho_0, t)$ given by (111) so that

$$H_Z(\rho, t) = H_{Z_1}(\rho, t) + H_{Z_3}(\rho, t) \quad (113)$$

where $H_{Z_1}(\rho, t)$ is given, as before, by (42) with $\xi = \pi/2$, while

$$H_{Z_3}(\rho, t) = -\epsilon_0 E_0 \int_0^d d\rho_0 \hat{G}_3(\rho, \rho_0, t) * \delta(t - \frac{v_0}{c}) \quad (114)$$

Substituting (112) in (114) we obtain

$$H_{z_3}(\rho, t) = \frac{E_0}{\pi Z_0} I \quad (115)$$

where

$$I = \int_0^d d\rho_0 ((ct)^2 - (\rho + \rho_0)^2)^{-1/2} U[ct - \rho - \rho_0] \quad (116)$$

A decomposition of this integral is

$$I = \{U[ct - \rho] - U[ct - (\rho + d)]\} \int_0^{ct-\rho} d\rho_0 ((ct)^2 - (\rho + \rho_0)^2)^{-1/2} \\ + U[ct - (\rho + d)] \int_0^d d\rho_0 ((ct)^2 - (\rho + \rho_0)^2)^{-1/2} \quad (117)$$

Written in this form, I is readily evaluated as

$$I = [U[\tau - (1 - \alpha)] - U[\tau - (2 - \alpha)]] \arccos((1 - \alpha)/\tau) \\ + U[\tau - (2 - \alpha)] [\arcsin((2 - \alpha)/\tau) - \arcsin((1 - \alpha)/\tau)] \quad (118)$$

where from (43), $\tau = (ct)/d$, and α is defined in (46). Using (72), (73), and (74) we obtain

$$j = j_1 + j_3 \quad (119)$$

where j_1 is the first two terms in (75) with $\xi = \pi/2$ and j_3 is given by

$$j_3 = (-1/\pi)I \quad (120)$$

with I given in (118). We can now write an explicit expression for j as

$$j = 1/\pi U(\tau - \alpha) \arccos(\alpha/\tau) + 1/\pi U(\tau - (2 - \alpha)) \arccos((1 - \alpha)/\tau) \\ - 1/\pi U(\tau - (2 - \alpha)) [\arcsin((2 - \alpha)/\tau) - \arcsin((1 - \alpha)/\tau)] \quad (121)$$

Using the relation

$$\arccos x + \arcsin x = \pi/2 \quad (122)$$

two times, we can write our final expression for j as

$$j = 1/\pi U(\tau - \alpha)\arccos(\alpha/\tau) + 1/\pi U(\tau - (2 - \alpha))\arccos((2 - \alpha)/\tau) \quad (123)$$

It is interesting to note that j given in (123) is exactly j_1 evaluated at $\xi = \pi/2$ and d replaced by $2d$. The reason for this, is that image theory could be applied to make the case treated in this section into a coplanar problem with a termination sheet having length $2d$.

V. Change of Variables to Obtain Solution When
Angle of Upper Flange is Varied

The analysis contained in this section is facilitated by referring to figure 3. This is essentially figure 1 viewed upside down. We orient our coordinate system in this manner so that we will be able to readily use the results contained in the previous sections. All of the previous results used (21) which we repeat here

$$H_z(\rho) = \int_0^d G(\rho, \rho_0) \sin \xi \epsilon_0 F \left[\frac{\partial E_y}{\partial t} \right] d\rho_0$$

When E_y given by (24) which is

$$\frac{E_y}{\rho} = -\hat{a}_y E_0 U \left(t - \frac{v_0}{c} \cos \xi \right)$$

was substituted into (21), then (26) was obtained. Performing the indicated convolution in (26) we obtain

$$H_z(\rho, t) = -\epsilon_0 E_0 \sin \xi \int_0^d d\rho_0 \hat{G}(\rho, \rho_0, t - \frac{v_0}{c} \cos \xi) \quad (124)$$

In the derivation of (21) it did not matter whether ξ was greater than or less than $\pi/2$. We are always interested in the case $\xi \leq \pi/2$ so that, referring to figure 3, $\xi' \geq \pi/2$. Equation (21) is valid for the situation depicted in figure 3 with all geometrical variables, t excluded, replaced by the appropriate primed variables. That is

$$H_z(\rho') = \int_0^d d\rho'_0 G(\rho', \rho'_0) \sin \xi' \epsilon_0 F \left[\frac{\partial E_{y'}}{\partial t'} \right] \quad (125)$$

In this primed coordinate system, the incident electric field is given by

$$E_{y'} = E_0 U \left(t + (\rho'_0/c) \cos \xi' \right) \quad (126)$$

The time, t , has exactly the same meaning as before. Substituting (126) into (125) and taking the inverse Fourier transform we obtain

$$H_z(\rho') = \epsilon_0 E_0 \sin \xi' \int_0^d d\rho'_0 \hat{G}(\rho', \rho'_0, t + (\rho'_0/c) \cos \xi') \quad (127)$$

Using the relation

$$\rho'_0 = d - v'_0 \quad (128)$$

and introducing the definition

$$t' = t + (d/c)\cos \xi' \quad (129)$$

we obtain

$$H_{z'}(\rho') = \epsilon_0 E_0 \sin \xi' \int_0^d d\rho'_0 \hat{G}(\rho', \rho'_0, t' - \frac{v'_0}{c} \cos \xi') \quad (130)$$

Because of the orientation of the primed and unprimed coordinate systems, \hat{a}_z and $\hat{a}_{z'}$, are oppositely directed. So (130) can be written as

$$H_z(\rho') = -\epsilon_0 E_0 \sin \xi' \int_0^d d\rho'_0 \hat{G}(\rho', \rho'_0, t' - \frac{v'_0}{c} \cos \xi') \quad (131)$$

Comparing (124) and (131) we see that we can use all of the results for varying the angle of the bottom flange in a simple manner to describe the effect of varying the angle of the top flange. We need only make the substitutions

$$\xi \rightarrow \xi' = \pi - \xi \quad (132)$$

$$\rho \rightarrow \rho' = d - \rho = v \quad (133)$$

$$t \rightarrow t' = t + (d/c)\cos \xi' \quad (134)$$

We will now show that substitution (134) is unnecessary. The only time dependence for the lower flange results appeared in the form of τ given in (43) by

$$\tau = \frac{ct - v \cos \xi}{d \sin \xi}$$

Accordingly, the t' dependence for the upper flange case is

$$\tau' = \frac{ct' - v' \cos \xi'}{d \sin \xi'} \quad (135)$$

We now substitute the relation

$$v' = d - \rho' \quad (136)$$

as well as (132), (133), and (134) into (135) in order to arrive at the conclusion

$$\tau' = \tau \quad (137)$$

In view of (137) we need not make the change of variables indicated in (134). In order to arrive at the upper flange solution we need only perform the substitution indicated by (132) and (133). That is replace ξ by $\pi - \xi$ and α by $1 - \alpha$ in all of the lower flange solutions. The substitution involving α comes from dividing all quantities appearing in (133) by d . We will now perform these substitutions and present our results for j when the angle of the upper flange is varied. For the general case it is

$$\begin{aligned} j = & 1/\pi U(\tau - \tau_1) \arccos[\tau^{-1}((1 - \alpha)\sin \xi + \tau \cos \xi)] \\ & + 1/\pi U(\tau - \tau_2) \arccos[\tau^{-1}(\alpha \sin \xi - \tau \cos \xi)] \\ & + q/\pi^2 \sin q\pi \{ [U(\tau - \tau_2) - U(\tau - \tau_3)] I_A + U(\tau - \tau_3) I_B \} \end{aligned} \quad (138)$$

where

$$\tau = \frac{ct - v \cos \xi}{d \sin \xi} \quad (139)$$

$$\tau_1 = (1 - \alpha) \frac{1 + \cos \xi}{\sin \xi} \quad (139)$$

$$\tau_2 = \alpha \frac{1 - \cos \xi}{\sin \xi} \quad (140)$$

$$\tau_3 = \tau_2 + \frac{1 + \cos \xi}{\sin \xi} \quad (141)$$

$$q \equiv 1/v = \pi/(\xi + \delta) \quad (142)$$

$$I_A = \int_0^1 A(y) \arccos g(y) dy \quad (143)$$

$$I_B = I_{B_1} + I_{B_2} \quad (144)$$

$$I_{B_1} = \int_0^{y_I} A(y) \arccos g(y) dy \quad (145)$$

$$I_{B_2} = \int_{y_I}^1 A(y) \{ \arcsin [g(y) + e(y)] - \arcsin g(y) \} dy \quad (146)$$

$$A(y) = 2y^{q-1} / (y^{2q} - 2y^q \cos q\pi + 1) \quad (147)$$

$$g(y) = C(C^2 + D^2)^{-1/2} \quad (148)$$

$$C = y^2 + 2y\beta \cos \xi + 1 \quad (149)$$

$$D^2 = 4y^2(\beta^2 - 1)\sin^2 \xi \quad (150)$$

$$e(y) = 2y \sin^2 \xi / [\alpha(C^2 + D^2)^{1/2}] \quad (151)$$

$$\beta = \tau(\sin \xi) / \alpha + \cos \xi \quad (152)$$

$$y_I = 1 + \Gamma - ((1 + \Gamma)^2 - 1)^{1/2} \quad (153)$$

$$\Gamma = [(\alpha\beta - \cos \xi)^2 - (1 + \alpha)^2] / (2\alpha) \quad (154)$$

It should be noted that the first term in (75) is the second term in (138) and the second term in (75) is the first term in (138). Thus, the coplanar contribution to the surface current density is the same for upper or lower flange bending, as it should be.

We now will present the solution when the observation point is at the bend. Previously, this corresponded to $\alpha = 1$ and now it corresponds to $\alpha = 0$. It is

$$j = \frac{1}{\pi} \left\{ U(\tau) \left[\pi - \xi + \frac{(\delta + \xi - \pi)\xi}{\xi + \delta} \right] + U(\tau - \tau_1) \arccos(\tau^{-1}(\sin \xi + \tau \cos \xi)) \left(1 - \frac{\delta + \xi - \pi}{\xi + \delta} \right) \right\} \quad (155)$$

where τ_1 is given in (139).

VI. Results

We obtain the values of inductance by comparing the ideal surface current density that we have calculated, with an approximate surface current density in an R, L admittance sheet. The approximate surface current density, j , was calculated by Baum [1] and is given by

$$j = [1 - \exp(-\tau/\beta)]U(\tau) \quad (156)$$

where the τ is the same one used in (43)

$$\tau = \frac{ct - v \cos \xi}{d \sin \xi}$$

and

$$\beta = \frac{l}{\sin \xi} \frac{c}{h} \frac{L}{Z_0} \quad (157)$$

In (157), c is the speed of light, h is the distance between the parallel plates, Z_0 is the free space wave impedance, ξ is the same angle used throughout this note, and L is the inductance to be calculated once β is known. Using the relation $c/Z_0 = 1/\mu_0$ where μ_0 is the magnetic permeability of free space, we can express L as

$$L = \mu_0 h \beta \sin \xi \quad (158)$$

so that once β is determined, L is also determined. In view of (158) we can consider β as a normalized value of inductance.

The procedure we used for determining β is as follows. We plotted the ideal surface current density versus τ for various ξ , δ , and α . We then plotted j_β versus τ on the same graph for a value of β which caused j_β to approximate the ideal surface current density, j , over a range of τ having practical interest. The lower limit of τ is chosen to be 0 despite the fact that the ideal current does not start at $\tau = 0$. The reason for this lower limit is that any real current would start at $\tau = 0$. The upper limit, $\tau = 3$, is chosen because this corresponds to matching the currents for a real time corresponding to $3(h/c)$ and this is considered sufficiently long to decide on the value of a component,

L, that is designed to perform for early times. In figures 4 through 16 we present the curves that lead to the choice of the β 's that appear in the following tables.

Table 1

$$\xi = \pi/2$$

$\delta \backslash \alpha$	0	.1	.5	.9	1.0
	Lower Flange β 's				
0	1.8	1.8	1.9	1.9	1.8
$\pi/6$	1.3	1.3	1.5	1.5	1.5
	Upper Flange β 's				
π	.9	.9	1.0	1.0	1.0

Table 2

$$\xi = \pi/3$$

$\delta \backslash \alpha$	0	.1	.5	.9	1.0
	Lower Flange β 's				
0	1.6	1.6	1.5	1.4	1.4
$\pi/6$	1.1	1.1	1.2	1.1	1.1
$\pi/3$	1.1	1.2	1.1	1.0	1.0
π	.9	1.0	.9	.7	.7
	Upper Flange β 's				
π	1.0	1.0	1.0	.9	.9

Table 3

$$\xi = \pi/4$$

$\delta \backslash \alpha$	0	.1	.5	.9	1.0
	Lower Flange β 's				
0	1.1	1.1	1.3	1.2	1.1
$\pi/6$	1.0	1.0	1.2	1.0	1.0
π	.9	1.1	.9	.7	.6
	Upper Flange β 's				
π	1.0	1.1	1.0	.9	.9

Table 4

$$\xi = \pi/10$$

$\delta \backslash \alpha$	0	.1	.5	.9	1.0
	Lower Flange β 's				
π	.6	.7	.8	.5	.5

In table 2 we included the coplanar case, $\delta = \pi/3$, because reference [1] did not include $\delta = \pi/3$. In table 4 we only included one flange orientation, $\delta = \pi$, because for $\xi = \pi/10$, the data for the ideal current was extremely close to the data presented in reference [1]. Even for $\delta = \pi$, the ultimate choice of β is the same one would obtain by considering coplanar data; however, a slight effect can be seen by comparing figure 13 with Baum's coplanar data. In general it is found that as ξ decreased the effect of varying the flange angle made progressively less percentage difference between the coplanar ideal current and the ideal current corresponding to a bending of the flange.

Our final choice for the value of β appropriate to a given inclination angle, ξ , is based on the following argument. We believe that the expression for the approximate current given in (156) is likely to be a more valid expression near the center of the termination. In addition, it seems that if one had an exact expression for the current in an R,L termination rather than (156), one would choose to match the exact current and the ideal current calculated in

this note at $\alpha = .5$ in order to determine β . Thus, we considered only the cases corresponding to $\alpha = .5$ in deciding on our value of β for various ξ , δ orientations. In the presentation of the β 's for $\xi \leq \pi/10$ we use Baum's data [1], since for these angles, the coplanar ideal current can be used for deciding the value of β without concerning ourselves with the angles or even the presence of the flanges.

Table 5

ξ	no flanges*	perfectly conducting ground ($\delta = 0$)	ground removed ($\delta = \pi/6$)
$\pi/2$	$\beta = 1.0$	$\beta = 1.9$	$\beta = 1.5$
$\pi/3$.95	1.5	1.2
$\pi/4$.95	1.3	1.2
$\pi/10$.8	.8	.8
$\pi/20$.8	.8	.8
$\pi/40$.6	.6	.6

*The values in the "no flange" column are the average values of β corresponding to the removal of the top flange and the removal of the bottom flange.

The values of β presented in table 5 together with (158) determine the value of inductance. The value of the resistance to be used in the admittance sheet comes from late time arguments that are independent of flange considerations. For completeness, we take that result from Baum [1]

$$R = Z_0 \sin \xi \quad (159)$$

A general observation can be made concerning the results summarized in table 5. The values of inductance to be used in the termination when the ground that the simulator rests on is either nonconducting or perfectly conducting can be made closer to each other in either of two ways. We can either decrease ξ , or for large ξ , we can remove ground beyond the simulator.

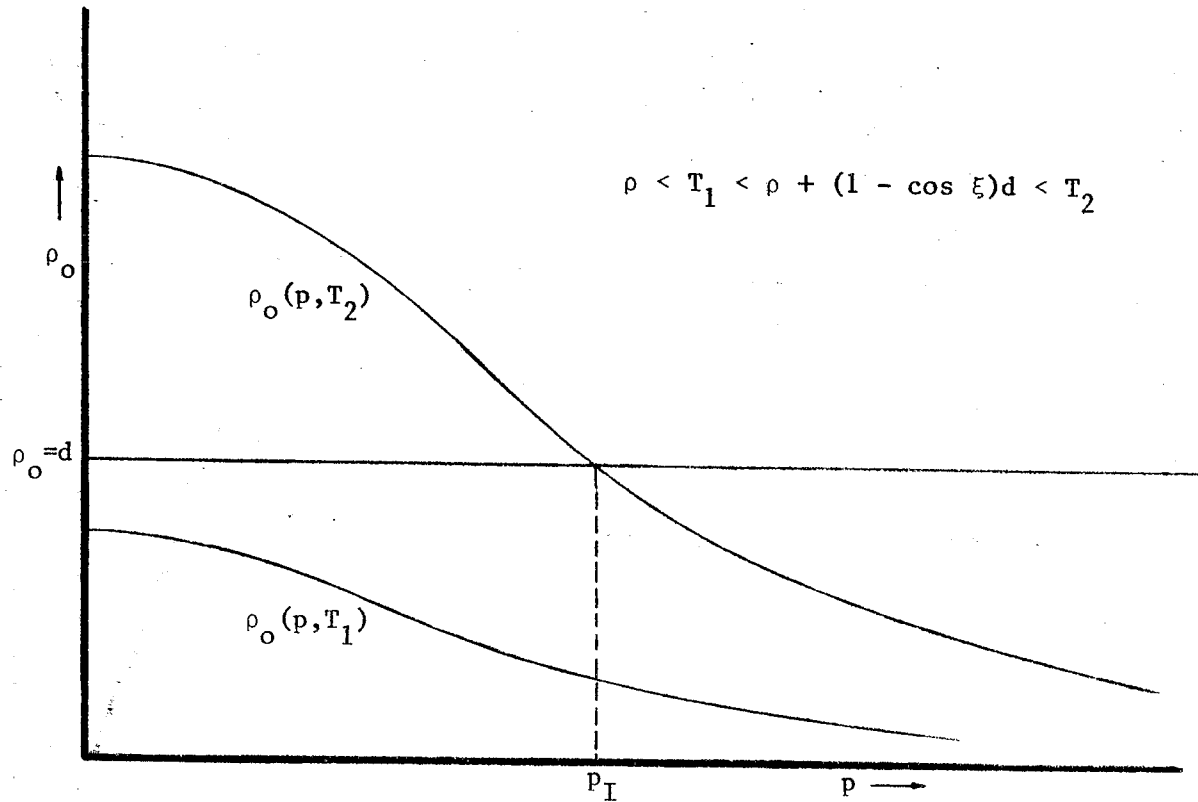


Figure 2. The ρ_0, p plane and appropriate curves for determining limits of integration.

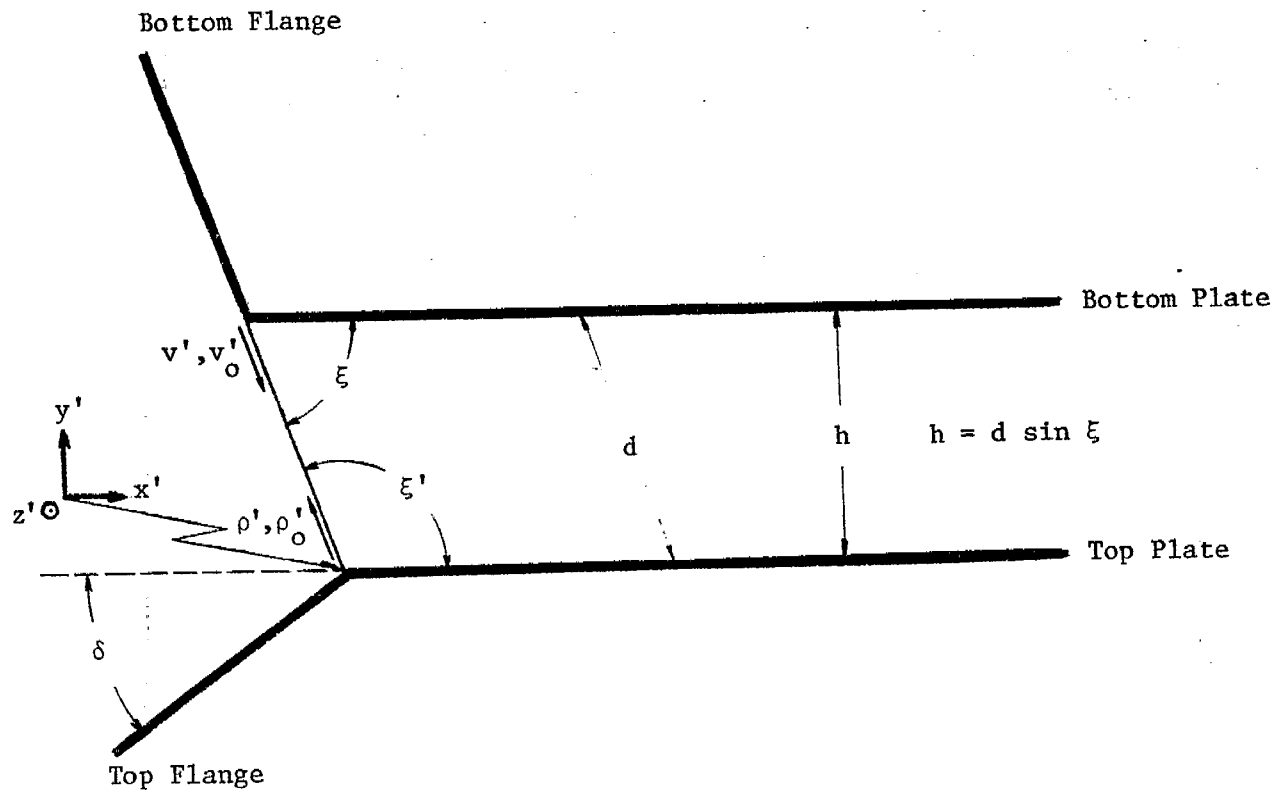


Figure 3. Geometry appropriate to varying the angle of the top flange.

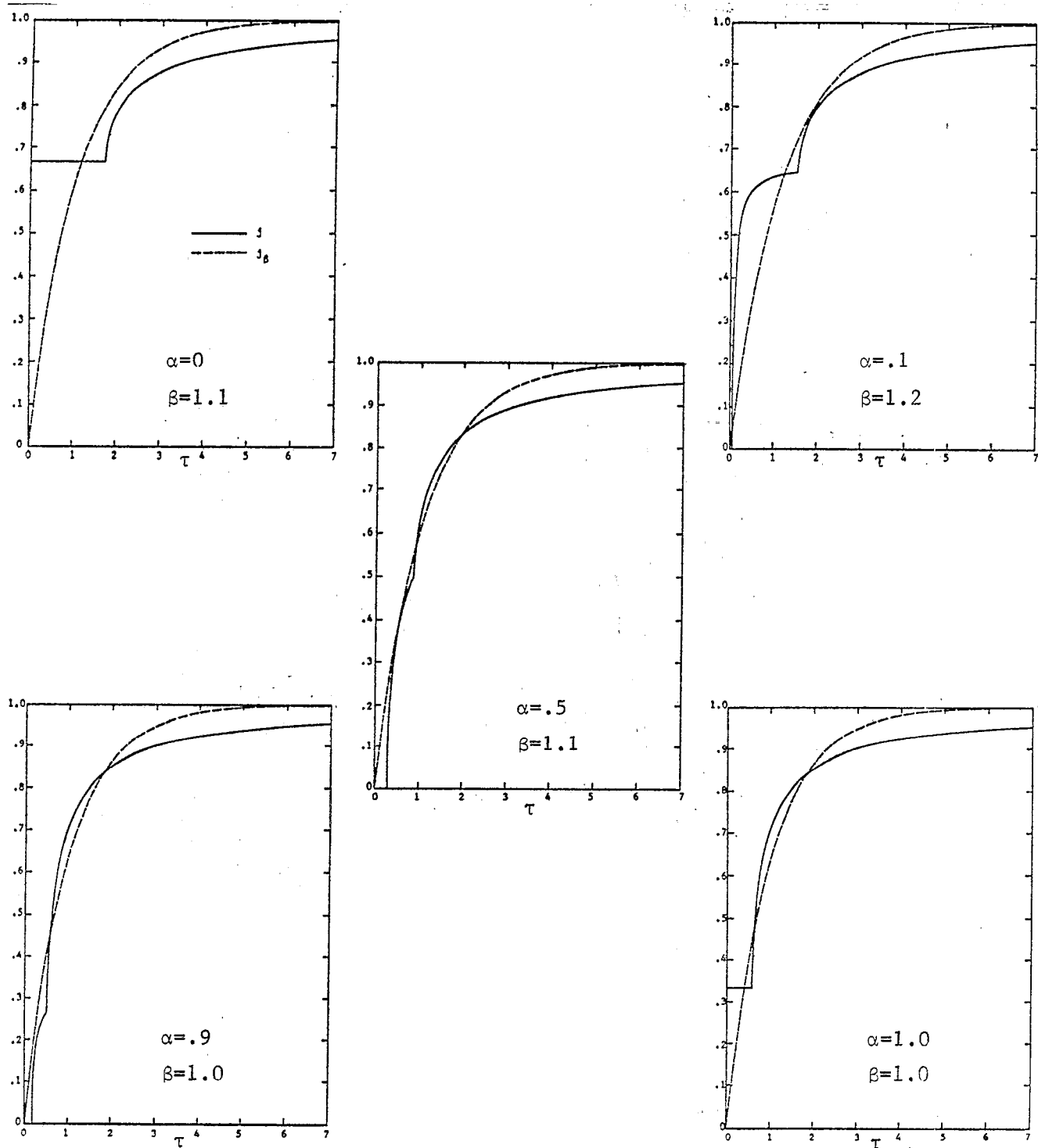


Figure 4. Ideal and approximate surface current densities versus normalized time at five points on the termination plane: $\xi = \pi/3$ and no bending of flanges.

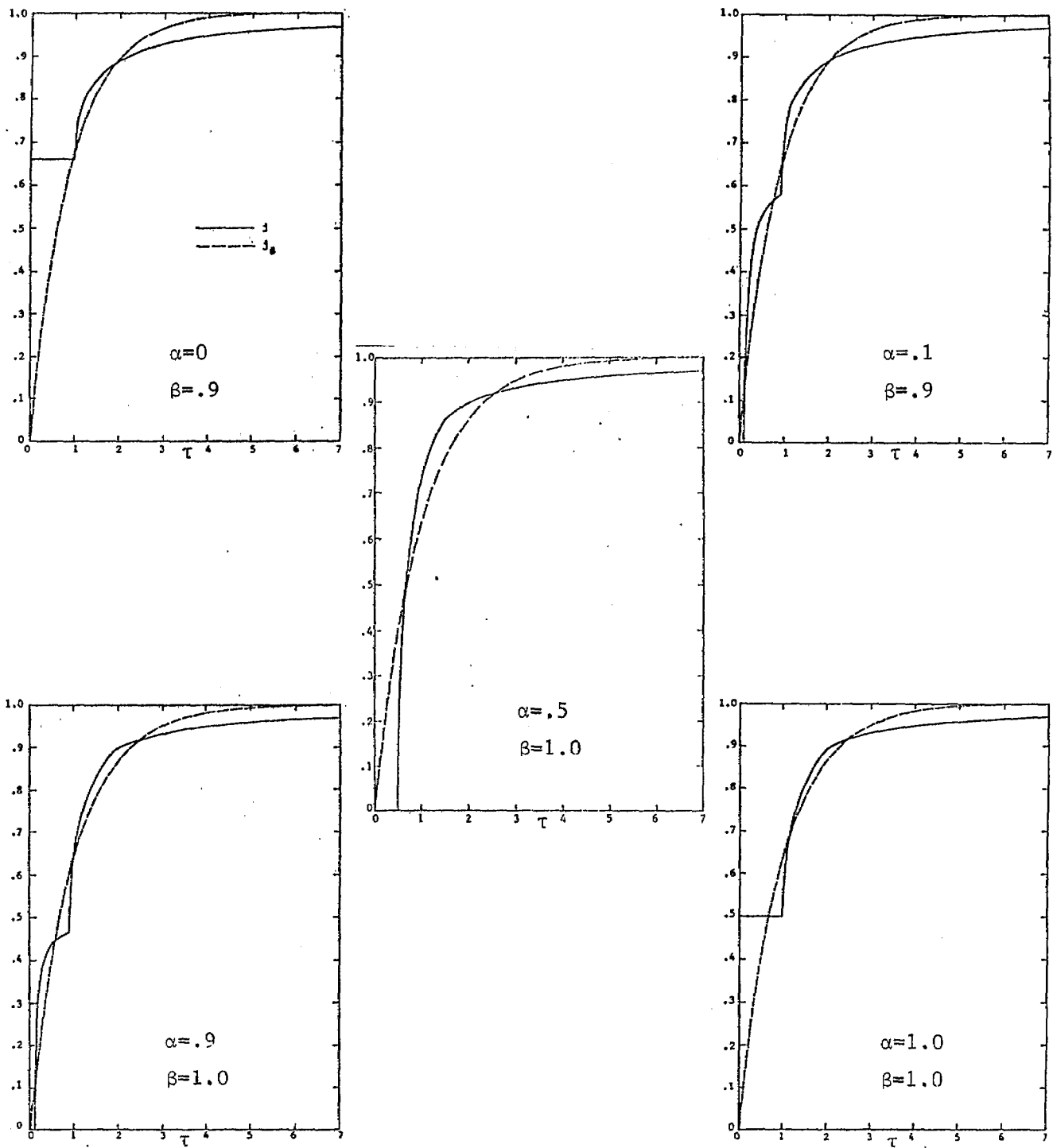


Figure 5. Ideal and approximate surface current densities versus normalized time at five points on the termination plane: $\xi = \pi/2$ and upper flange removed. Data also corresponds to $\xi = \pi/2$ and lower flange removed with the α 's appropriately interchanged.

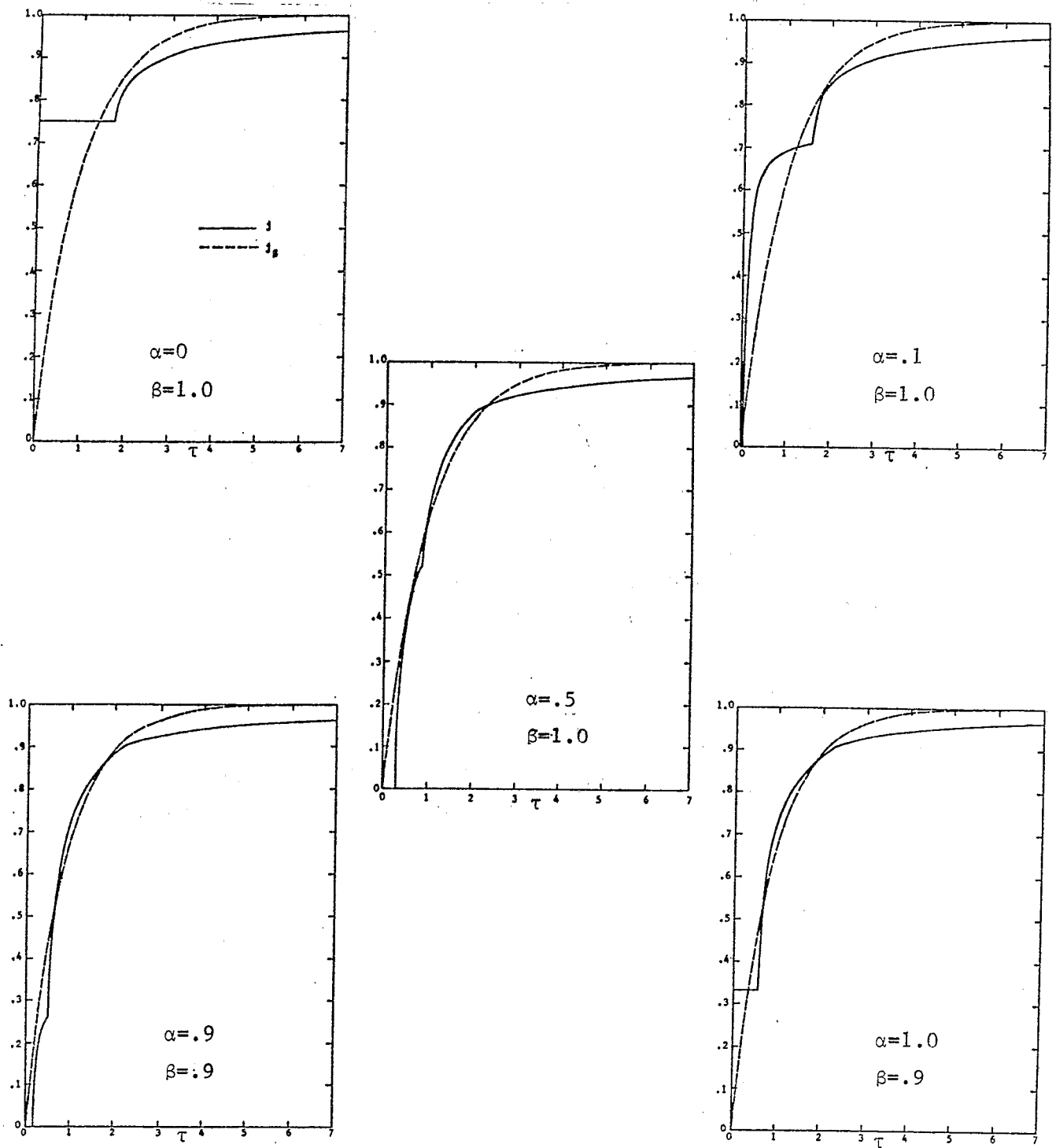


Figure 6. Ideal and approximate surface current densities versus normalized time at five points on the termination plane: $\xi = \pi/3$ and upper flange removed.

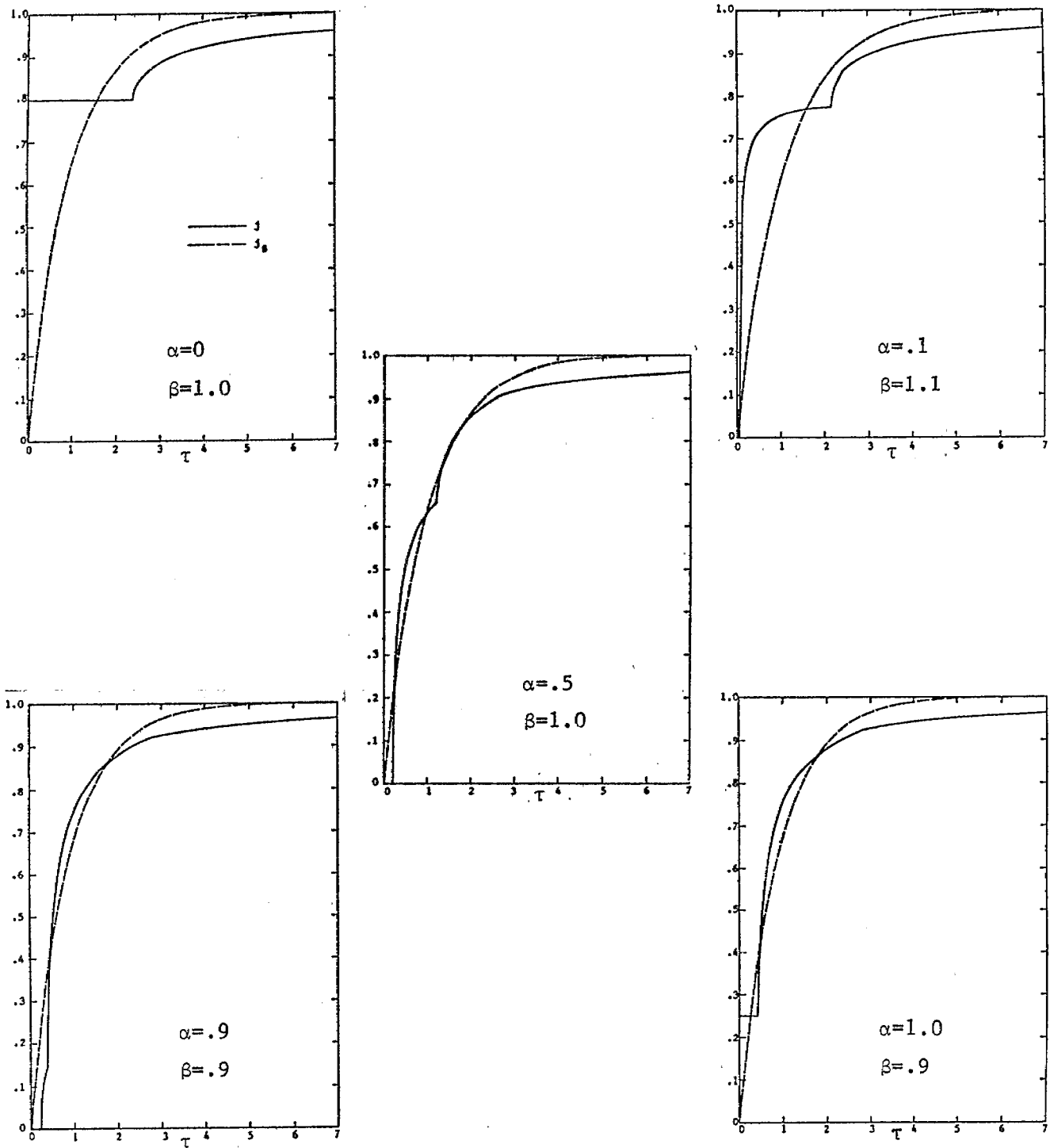


Figure 7. Ideal and approximate surface current densities versus normalized time at five points on the termination plane: $\xi = \pi/4$ and upper flange removed.

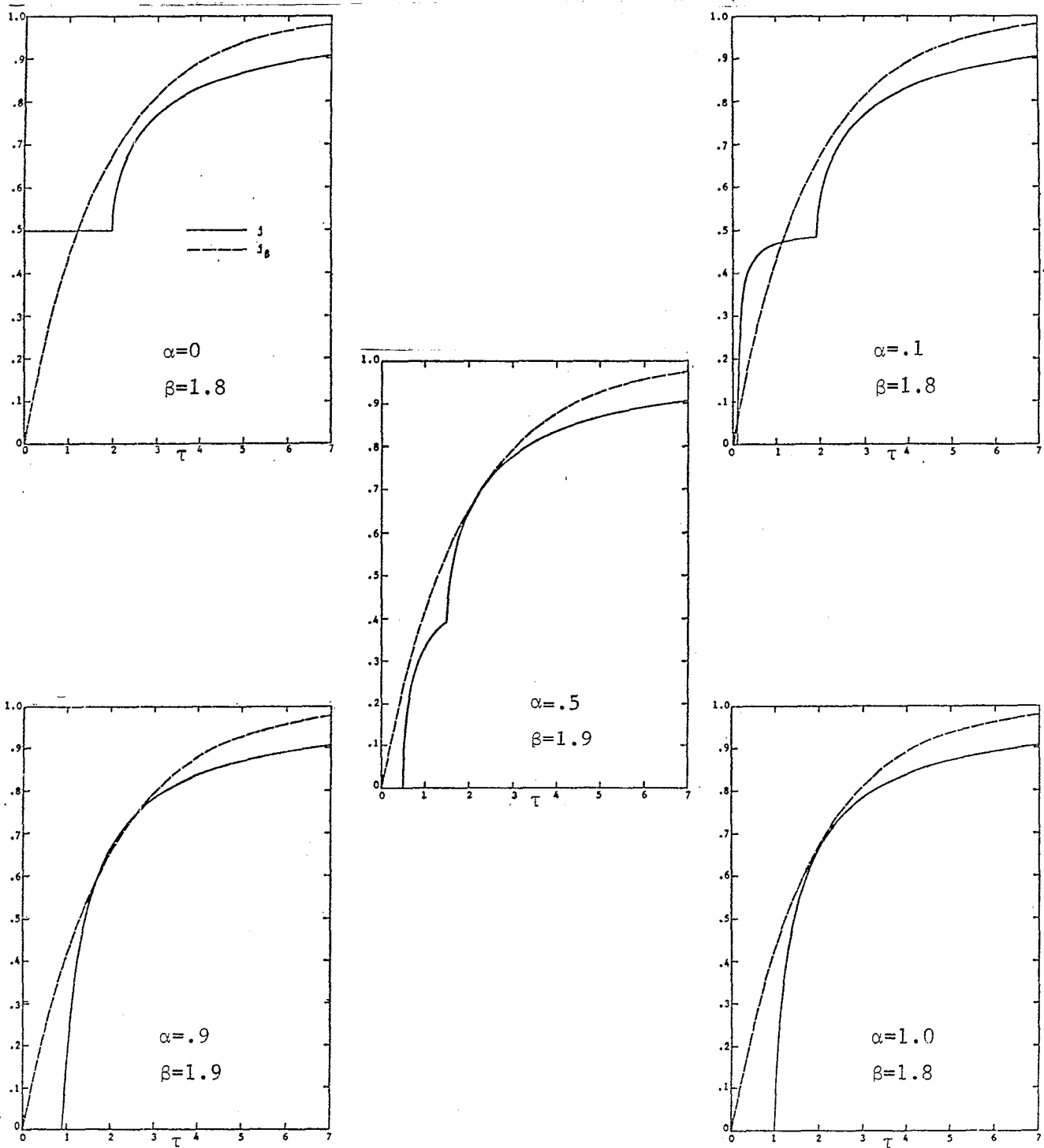


Figure 8. Ideal and approximate surface current densities versus normalized time at five points on the termination plane: $\xi = \pi/2$, $\delta = 0$ (lower flange).

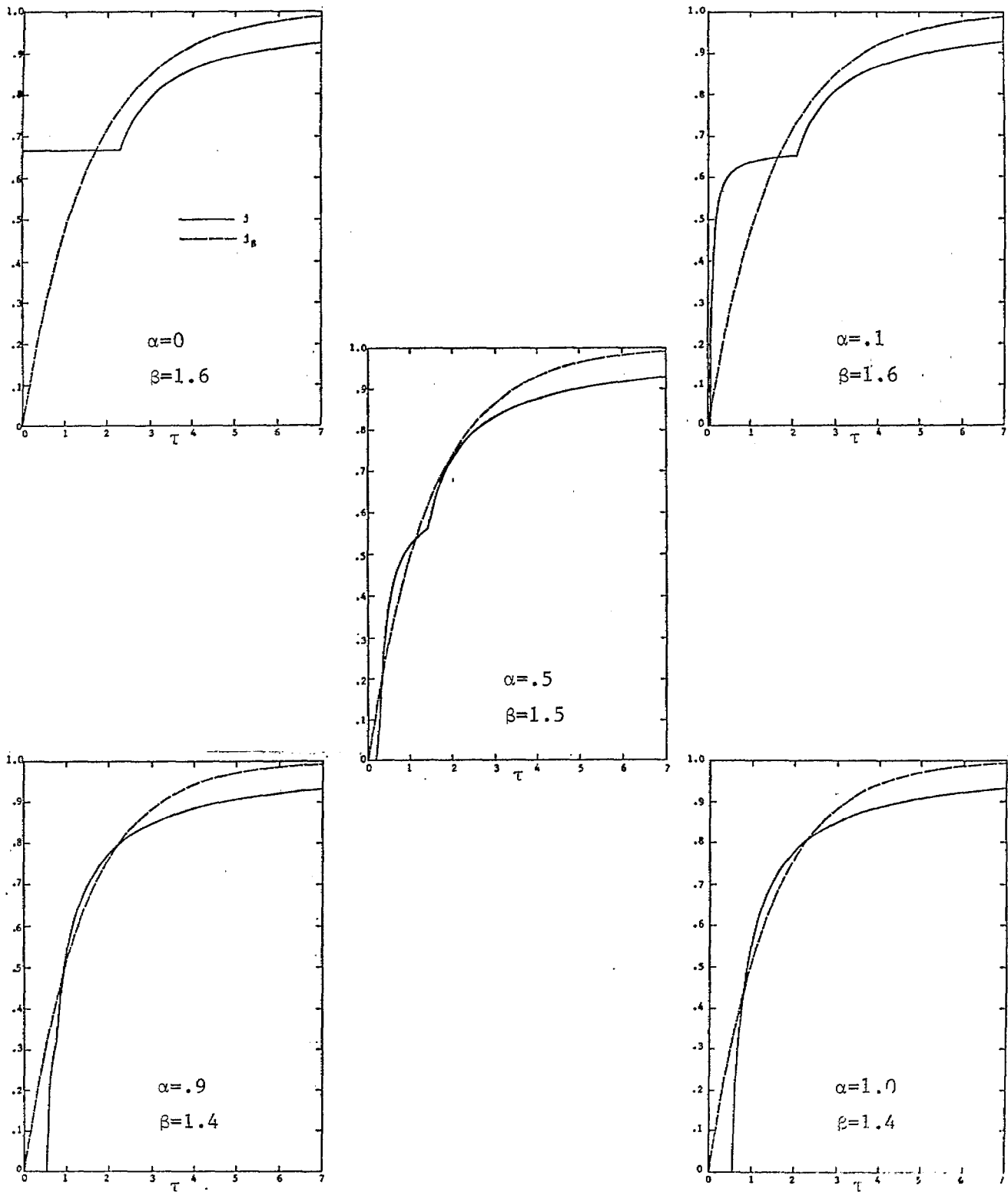


Figure 9. Ideal and approximate surface current densities versus normalized time at five points on the termination plane: $\xi = \pi/3$, $\delta = 0$ (lower flange).

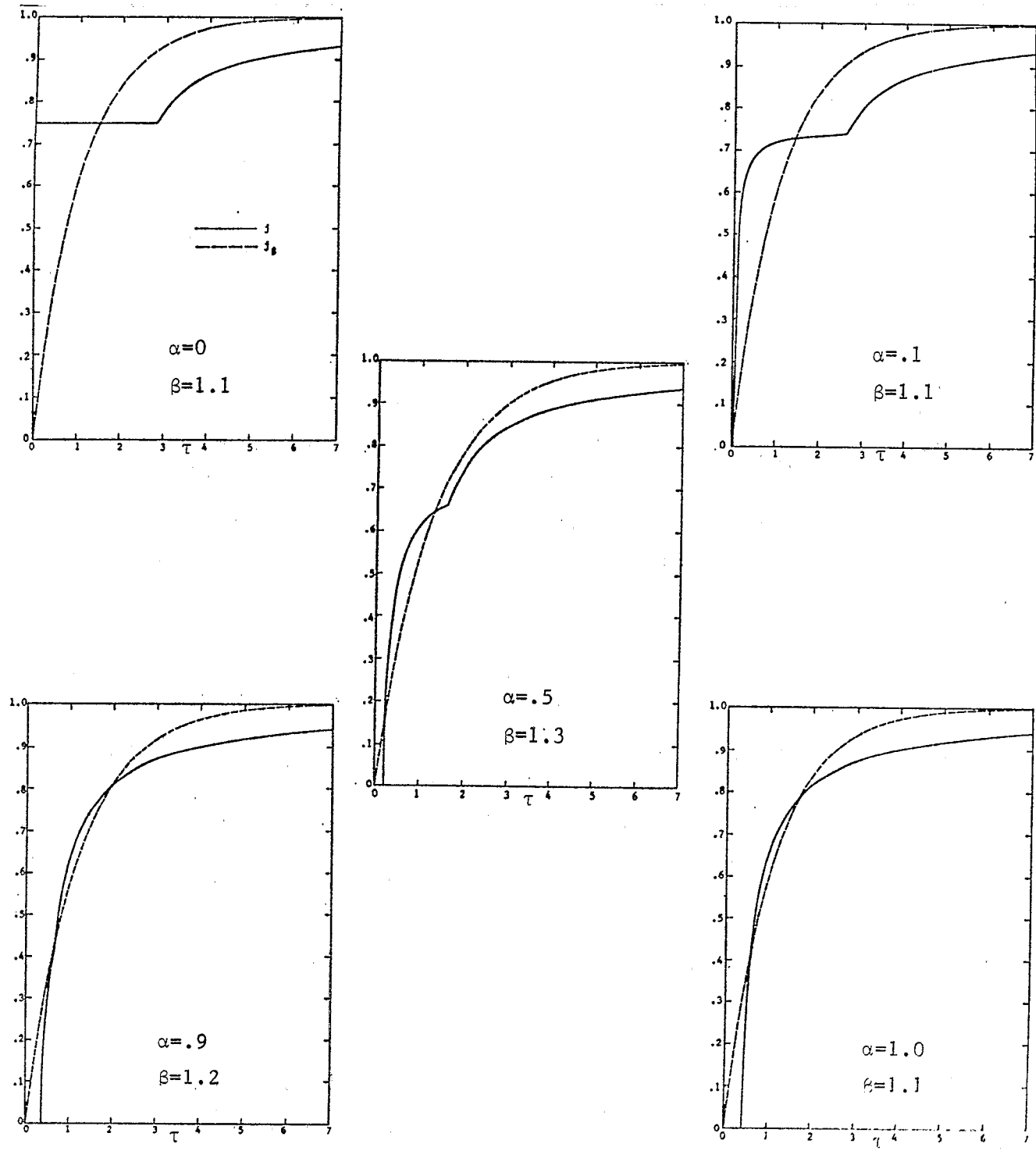


Figure 10. Ideal and approximate surface current densities versus normalized time at five points on the termination plane: $\xi = \pi/4$, $\delta = 0$ (lower flange).

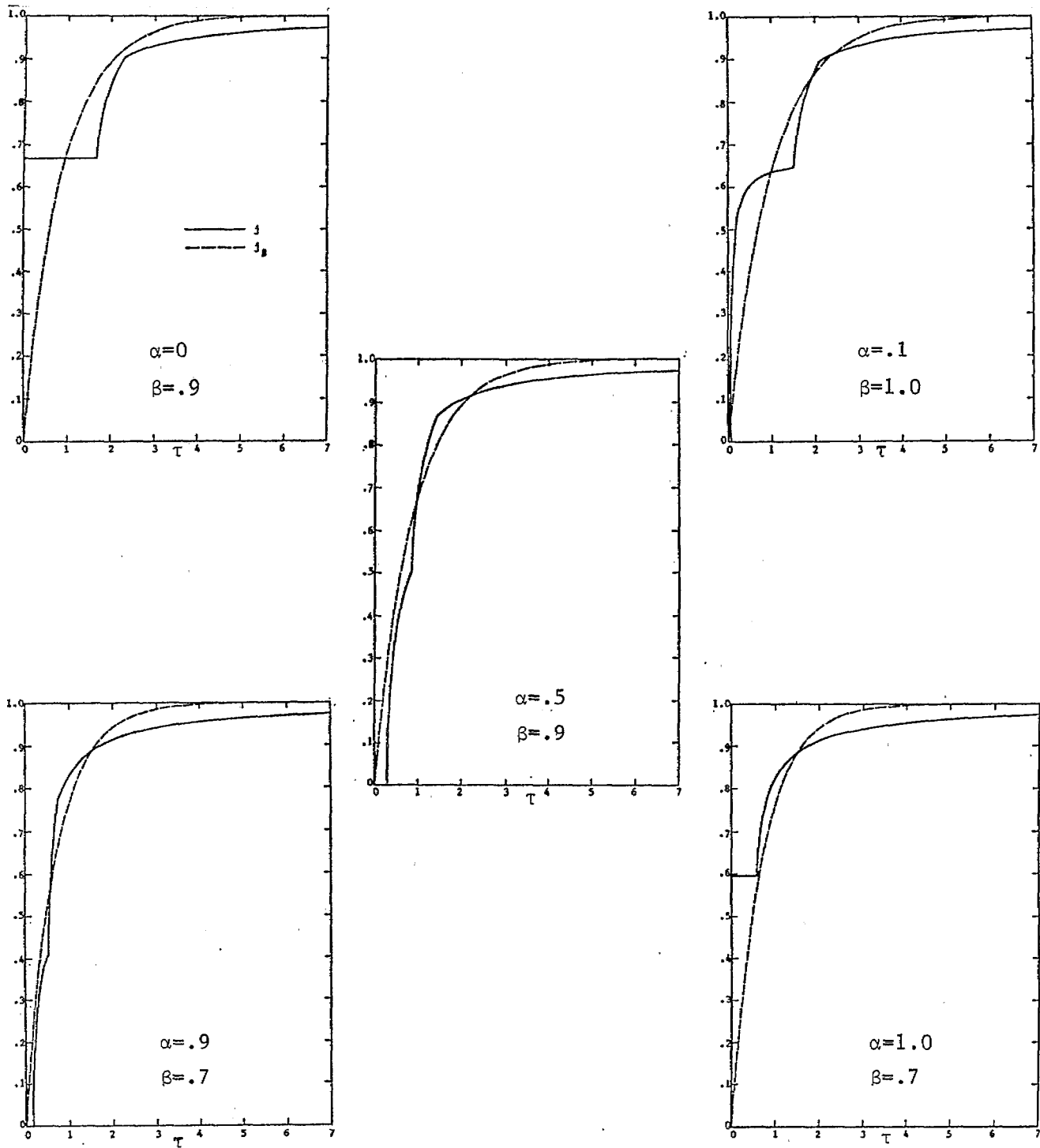


Figure 11. Ideal and approximate surface current densities versus normalized time at five points on the termination plane: $\xi = \pi/3$, $\delta = \pi$ (lower flange).

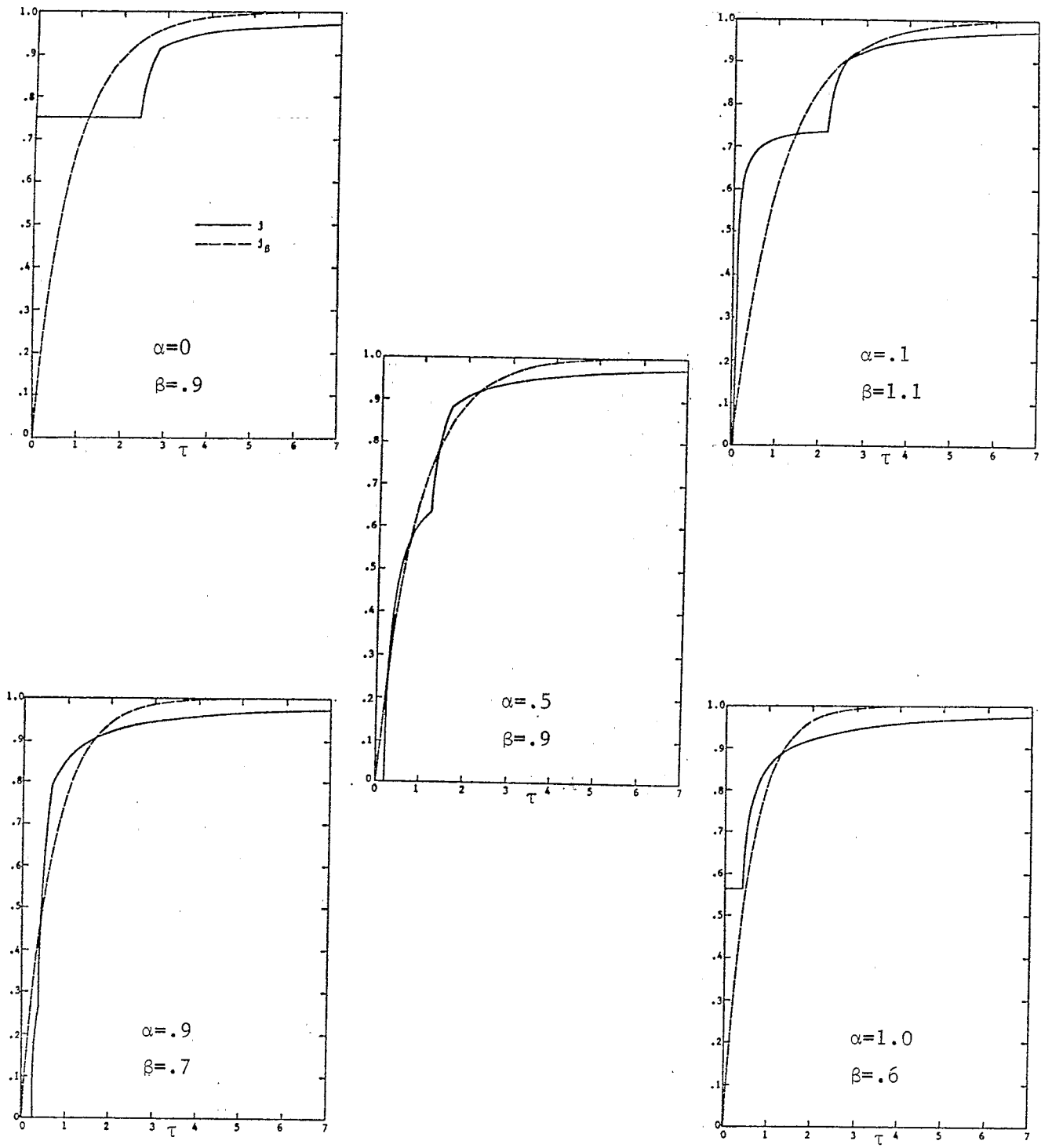


Figure 12. Ideal and approximate surface current densities versus normalized time at five points on the termination plane: $\xi = \pi/4$, $\delta = \pi$ (lower flange).

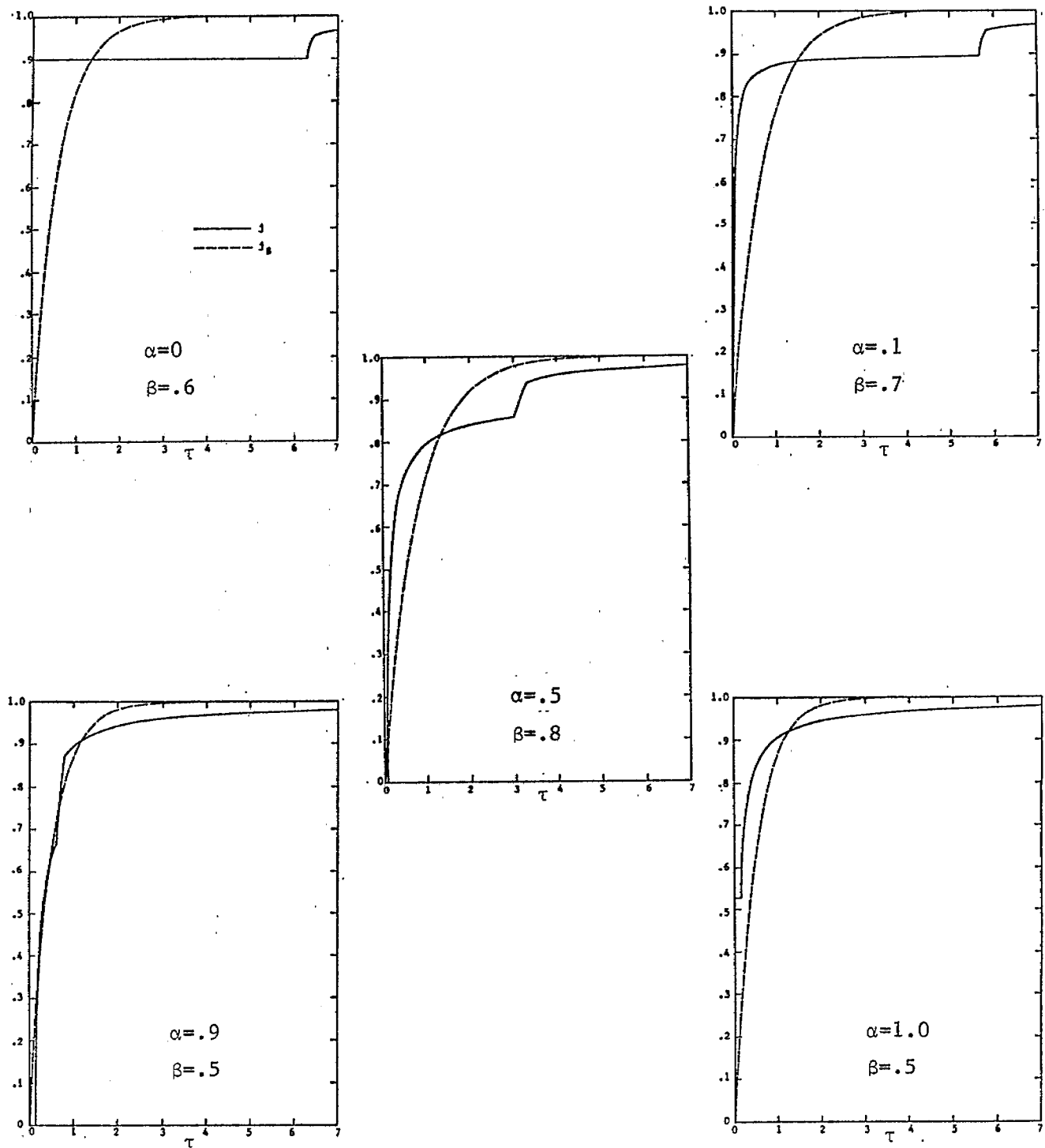


Figure 13. Ideal and approximate surface current densities versus normalized time at five points on the termination plane: $\xi = \pi/10$, $\delta = \pi$ (lower flange).

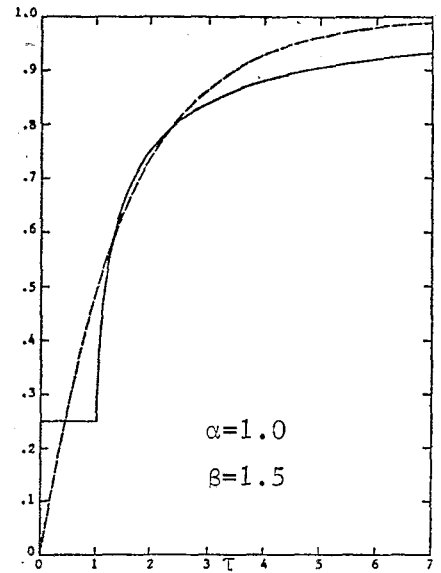
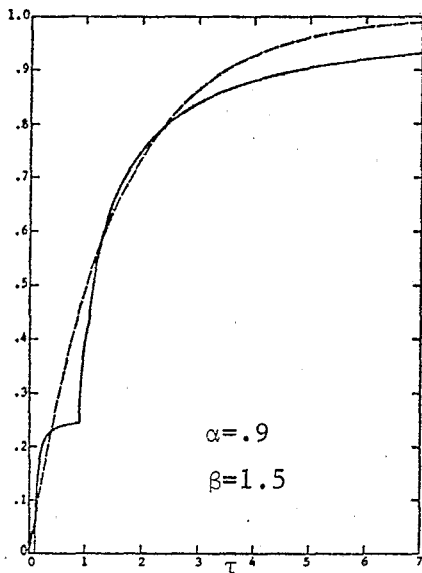
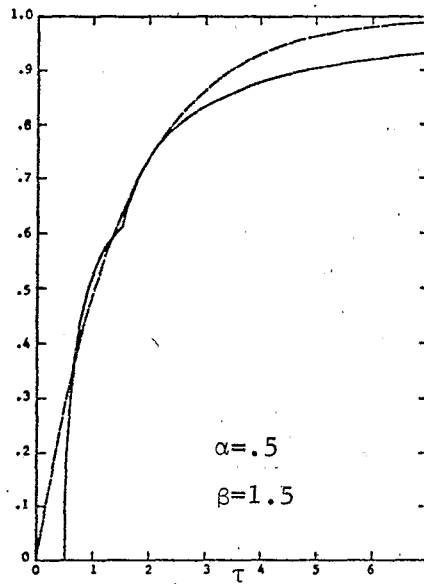
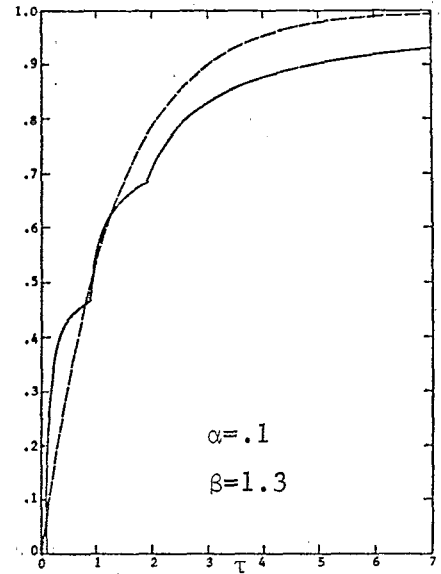
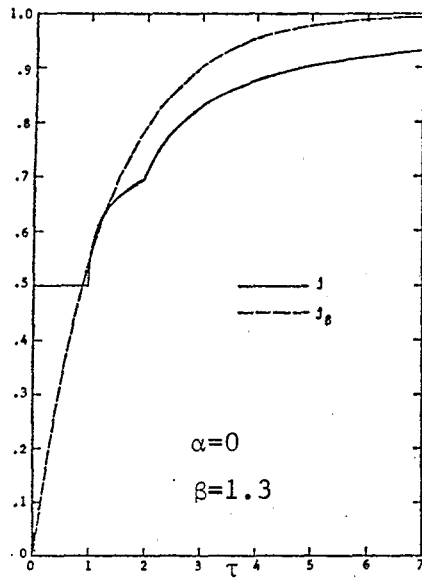


Figure 14. Ideal and approximate surface current densities versus normalized time at five points on the termination plane: $\xi = \pi/2$, $\delta = \pi/6$ (lower flange).

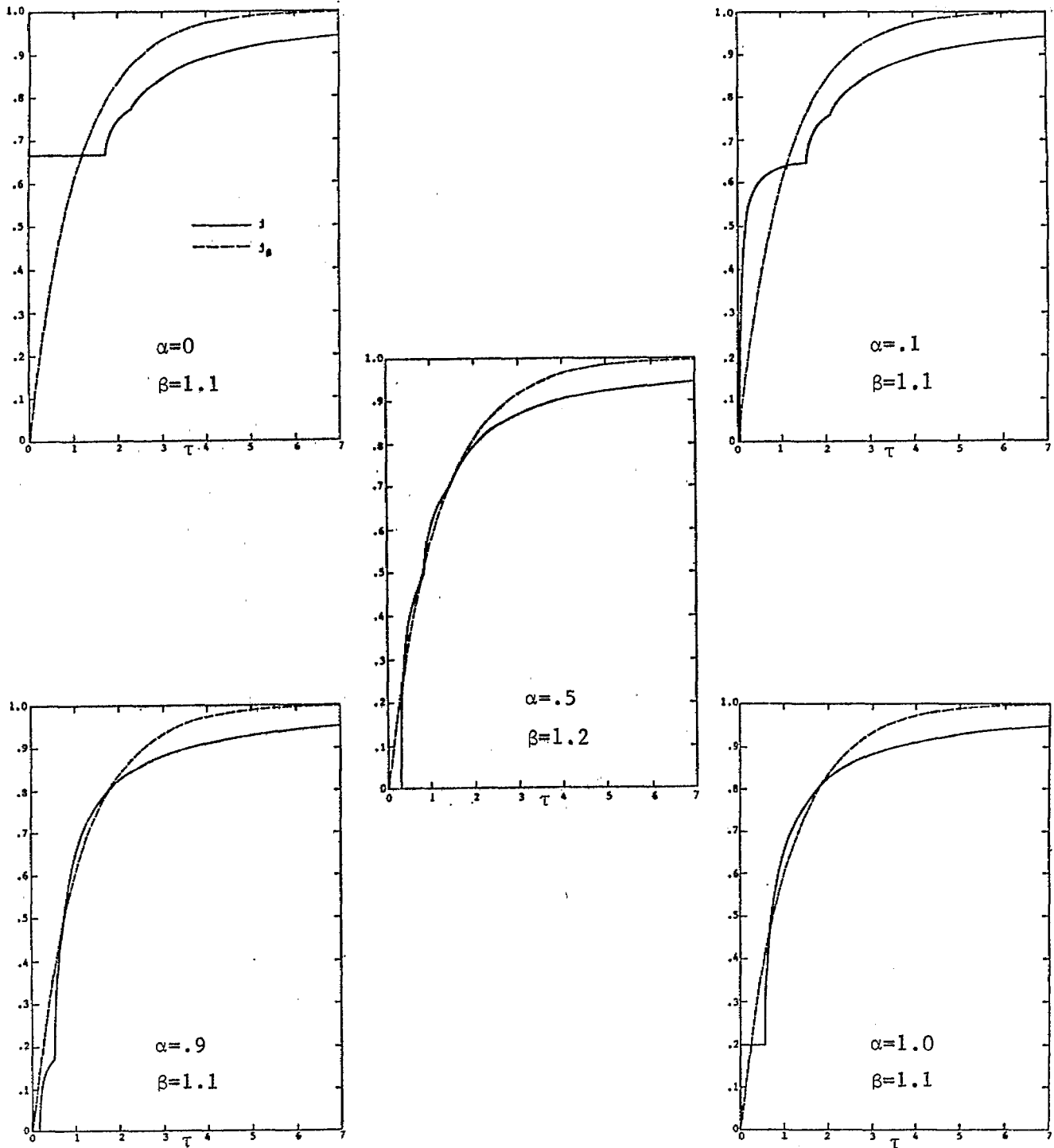


Figure 15. Ideal and approximate surface current densities versus normalized time at five points on the termination plane: $\xi = \pi/3$, $\delta = \pi/6$ (lower flange).

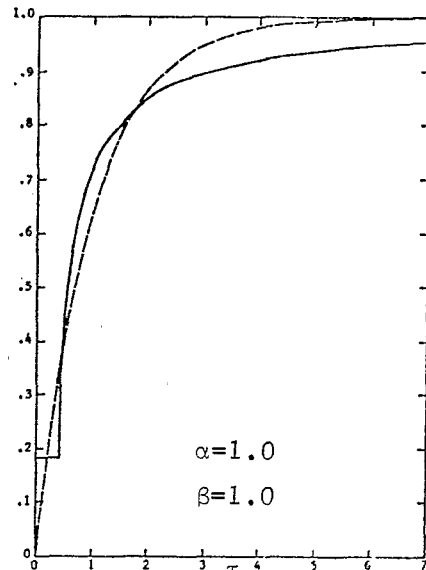
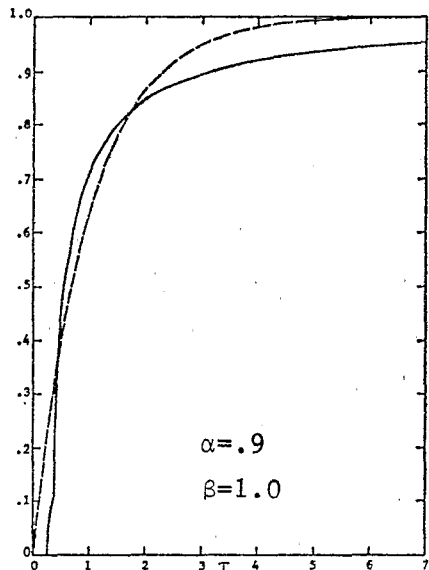
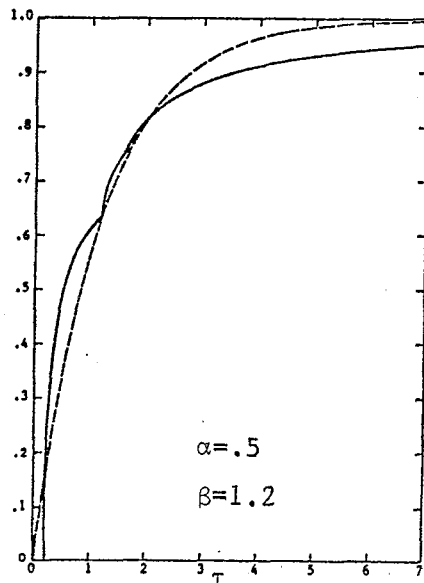
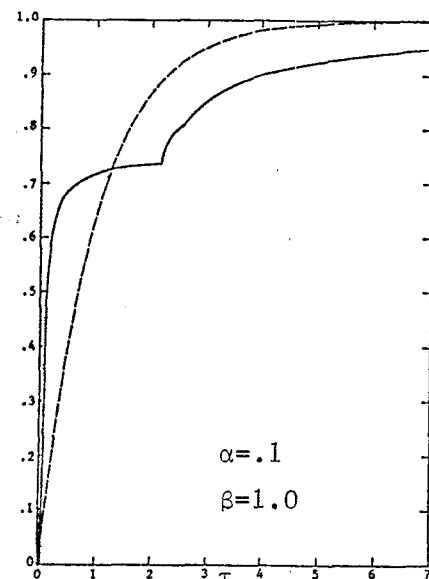
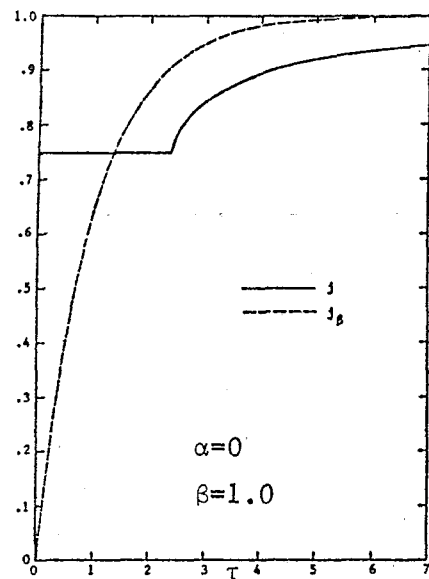


Figure 16. Ideal and approximate surface current densities versus normalized time at five points on the termination plane: $\xi = \pi/4$, $\delta = \pi/6$ (lower flange).

Acknowledgement

We thank Dr. C. E. Baum for suggesting this problem, Mr. R. W. Sassman for computer programming, and Mrs. G. Peralta for preparing this manuscript.

References

1. Capt. Carl E. Baum, "A sloped admittance sheet plus coplanar conducting flanges as a matched termination of a two-dimensional parallel-plate transmission line," *Sensor and Simulation Notes*, Note 95, December 1969.
2. J. J. Bowman, T. B. A. Senior, and P. L. E. Uslenghi, Electromagnetic and Acoustic Scattering by Simple Shapes, John Wiley and Sons, Inc., New York, p. 268, 1969.
3. P. M. Morse and H. Feshbach, Methods of Theoretical Physics, McGraw-Hill, Inc., New York, pp. 811 & 842, 1953.
4. Capt. Carl E. Baum, "A simplified two-dimensional model for the fields above the distributed-source surface transmission line," *Sensor and Simulation Notes*, Note 66, December 1968.